Seismic anisotropy inferred from direct S-waves derived splitting measurements and its geodynamic implications beneath southeastern Tibetan Plateau

Ashwani Kant Tiwari[1], Arun Singh[1], Tuna Eken[2], and Chandrani Singh[1]

[1]Department of Geology and Geophysics, Indian Institute of Technology Kharagpur, India
[2]Department of Geophysical Engineering, Istanbul Technical University, Turkey

Correspondence to: Arun Singh (arun@gg.iitkgp.ernet.in)

Abstract. The present study deals with detecting seismic anisotropy parameters beneath southeastern Tibet near Namche Barwa Mountain using splitting of direct S-waves. We employ the reference station technique to remove the effects of source side anisotropy. Seismic anisotropy parameters, splitting time delays and fast polarisation directions were estimated through analyses on a total of 501 splitting measurements obtained from direct-S waves from 25 earthquakes ($\geq$5.5 magnitude) that recorded at 42 stations of Namchebarwa seismic network. We have observed a large variation in time delays ranging from 0.64 to 1.68s, but in most cases, it is more than 1s, which suggests a highly anisotropic lithospheric mantle in the region. A comparison between direct S- and SKS derived splitting parameters shows a close similarity although some discrepancies exist where null or negligible anisotropy is reported earlier using SKS. The seismic stations with null or no anisotropic measurements are now supplemented with new measurements having clear anisotropic signatures. Our analyses indicate a sharp change in lateral variations of fast polarisation directions (FPDs) from consistent SSW-ENE or W-E to NW-SE direction at the southeastern edge of Tibet. Comparison of the FPDs with global positioning system (GPS) measurements, absolute plate motion (APM) directions and surface geological features signify that the observed anisotropy and hence inferred deformation patterns are not only due to asthenospheric dynamics but is a combination of lithospheric deformation and sub-lithospheric (asthenospheric) mantle dynamics. Direct S-waves-based station averaged splitting measurements with increased back-azimuthal coverage tend to fill the missing links that remain rather elusive due to lack of SKS measurements.

1 Introduction

The Tibetan plateau has a long history of deformation within the last 50 million years (e.g., Rowley and Currie, 2006; Henderson et al., 2011). Reliability of seismic anisotropy measurements is a challenging issue as it is essential to identify the tectonics, coupling/decoupling of the crust-lithospheric mantle, multi-layered anisotropic modelling, and active seismicity in relation to the type of deformation and possible flow patterns, which are still a matter of debate in understanding the formation processes and future challenges of this active region.

Lattice preferred orientation (LPO) of olivine mineral in the mantle as a result of plate interactions are controlled by various geodynamic processes and is considered to be the main cause for the shear wave splitting observations on the teleseismic S and

SKS waves. Deformation in the upper mantle generally takes place through two processes, namely diffusion and dislocation creep under the favorable conditions. Dislocation creep process, which is the creeping motion of crystal dislocation, is considered to be the leading cause of developed anisotropy (Karato, 1987; Nicolas and Christensen, 1987; Karato and Wu, 1993; Mainprice et al., 2000). High-stress condition or large grain size or both cause it, but the nonlinear increase in the strain rate is independent of the grain size (Karato and Wu, 1993). This type of deformation is expected to occur at a depth range less than 400km (e.g., Karato, 1984, 1987) where olivine is the most common mineral and hence LPO development and observed anisotropy mainly represents upper 400km depth (Becker and Faccenna, 2011).

Several observations on seismic anisotropy have greatly contributed to elucidating these deformation patterns about the past and present geodynamic activity of the region. Generally speaking, SKS splitting analyses are the most diagnostic, quick, and well-established way of detection and quantification of seismic anisotropy. SKS phase does not propagate as S-wave in the liquid outer core and refract from P-wave into only SV (radial) component when entering the mantle of a receiver-side region. Hence a recorded SKS phase at the surface does not pose any influence of the source side anisotropy The main disadvantage of using SKS phase in splitting measurements is that finding good-quality observations is limited due to several parameters, i.e., epicentral distance and propagation direction of the event in most cases thus and need to be supplemented with other waves (e.g. ScS and direct-S) that can provide a better azimuthal coverage. However, employing such additional waves may introduce contamination of shear signal due to the dominant source-side anisotropy. Splitting of shear waves is similar to the birefringence phenomena in optics. Shear waves split into fast and slow components when they pass through an anisotropic media. In such situation, we obtain elliptical particle motion of horizontal components. If the anisotropy is the only cause for splitting then the observed shear wave (fast or slow) can be rotated in such a way that two very similar phases are seen apart from scaling and a time delay between them (Eken and Tilmann, 2014). Resultant splitting parameters ϕ and δt imply the rotation angle in relation to the flow direction and shearing or extension at a particular depth under the assumption of LPO in the upper mantle, and to the strength and thickness of the anisotropic layer, respectively. Splitting measurements from the Himalaya-Tibet collision zone have been explained with the presence of single homogeneous layer with a horizontal axis of the symmetry (e.g., McNamara et al., 1994; Chen et al., 2010; Sol et al., 2007; Herquel et al., 1995; Hirn et al., 1995; Lavé et al., 1996; Sandvol et al., 1997; Huang et al., 2000; Lev et al., 2006; Wang et al., 2008; Fu et al., 2008; Sato et al., 2012).

The use of direct-S waves of the earthquakes at teleseismic distance ranges (30°-90°) can provide complementary splitting measurements to previous ones as this helps in establishing a robust and coherent database that will be inferred from good-quality of S-wave signals from relatively enhanced azimuthal distribution. This is crucial for the Indian sub-continent where SKS measurements are skewed towards eastern azimuths and very few SKS measurements are obtained due to temporary deployments (see Singh et al., 2015). However, the major problem in including direct S-waves into splitting measurements is the contamination of the S-wave signals due to the influence of anisotropic structures existing within the source-side region. Eken and Tilmann (2014) have recently shown that this problem can be overcome using an array-based approach, Reference Station Technique (RST). The method assumes identical source-side anisotropy effect on closely located two stations (reference and target stations) with respect to the epicentral stations. In this case optimum splitting parameters can be estimated by searching for receiver-side correction parameters for the target station that result in maximum similarity to the S-wave signal

corrected for previously known receiver-side anisotropy beneath the reference station in a grid search scheme. Signals used for that comparison are that of the reference station previously corrected for known reference receiver-side anisotropy and of the target station whose receiver-side splitting parameters are desired to be estimated. In this technique, we have utilised seismic anisotropy parameters, which were previously inferred from the SKS measurements by Sol et al. (2007) as the reference knowledge of the receiver-side anisotropy beneath the reference station. The RST has been earlier successfully tested through both synthetic and observed data collected along the northeastern, southwestern parts of the Tibetan Plateau and the Hellenic Trench in eastern Mediterranean (e.g., Eken and Tilmann, 2014; Singh et al., 2016; Confal et al., 2016). Our study focuses on the south-east part of Tibet near Namche Barwa (Figure 1). The study region is located between and around the Indus-Tsangpo Suture Zone (ITSZ) and Bangong-Nuijiang Suture Zone (BNSZ). Our major motivation is to calculate S-wave derived seismic anisotropic parameters that may have a potential link to tectonic setting and deformation history with the help of a correlative analysis of resultant anisotropy observations with Absolute Plate Motion (APM) directions, GPS measurements and the structural and topographic features. Our study contradicts the isotropic nature of the Indian lithospheric mantle and adds new constraints in understanding the types of deformation and their causes in the region.

2 Tectonics of the region

The formation of Tibetan plateau and the Himalayan mountain belts are due to collision and post-collision processes of the Indian and Eurasian plates from 50 million years ago (Argand, 1924; Garzanti and Van Haver, 1988; Molnar and Tapponnier, 1975; Yin and Harrison, 2000; Royden et al., 2008). Underthrusting of the Indian lithosphere beneath the Eurasian lithosphere has been proposed to be the main reason for the formation of the Himalayan and Karakorum ranges (Nelson et al., 1996; Kumar et al., 2006; Tseng et al., 2009) along with the formation of the Central Tibetan region (Argand, 1924; Nelson et al., 1996; Li et al., 2008). Underlying reason for the development of the northern and eastern Tibetan plateau, however, remains still enigmatic (Karplus et al., 2011; Royden et al., 2008). McKenzie and Priestley (2008) discuss the development of the northern Tibetan lithosphere as an accreted one. Royden et al. (2008) argued that the Tibetan plateau has evolved due to the subduction of Indian lithosphere beneath Eurasia, which is also responsible for the thickening of Tibetan crust and afterwards extrusion of the Tibetan lithosphere towards the east.

Various models have been developed regarding the deformation of Tibet (Royden et al., 1997; Molnar and Tapponnier, 1975; Houseman and England, 1986, 1993, 1996; Tapponnier et al., 1982, 2001; Shen et al., 2001; Holt et al., 1995, 2000; Replumaz and Tapponnier, 2003; Flesch et al., 2001) but no single model can explain the whole. The debate is open to understand the crust and mantle deformation patterns and ongoing geodynamics. Multistage subduction (Jagoutz et al., 2015; Van Hinsbergen et al., 2012) of Tethys oceanic plate and Indian plate below the Eurasian plate results in highly heterogeneous and anisotropic lithosphere. The Tibetan and Himalayan region is mainly dominated by thrust and strike-slip faulting (Figure 1). Suture zones are extended in the E-W direction and take a sharp turn around Eastern Himalayan Syntaxis (EHS). Strike-slip faulting becomes more dominant to the east of the EHS. Figure 1 signifies that the eastern portion of the subducting Indian plate are found up to

the EHS (León Soto et al., 2012) where the structural and topographical features take a sharp trend from nearly W-E striking to N-S striking.

3 Data and Method

In this study, we used a total of 5285 waveforms of direct-S waves extracted from 161 teleseismic events with magnitudes $\geq$5.5 within an epicentral distance range from 30° to 90°. The teleseismic events used in this study are recorded at 47 seismic stations of the XE network, which was operated in between 2003-2004 (Sol et al., 2007) (Figure 2). Out of 47 stations, we have only selected those 36 seismic stations where we have knowledge of seismic anisotropy inferred from SKS splitting measurements performed by Sol et al. (2007) to be used when correcting for receiver-side anisotropy beneath the reference stations. Prior to the data analysis, we have removed the instrument response from the original seismograms to overcome biases that can depend on the potential use of different stations (at reference and target sites). At the stage of the preprocessing, a band-pass filter between 0.03 and 0.2 Hz was applied to enhance S signals and seismograms resampled at 20 samples per second to avoid aliased signals and to reconstruct the waveforms to appropriate frequency range. Signals with any possible contaminations with other phases such as ScS, SKKS, and SKS are omitted from the analysis. We selected only those waveforms with a signal to noise ratio (SNR) $\geq$2.5 on the transverse and radial components for further analysis. The selection of the waveforms is achieved by performing a visual inspection manually that allowed only 40% of the direct-S waveforms. All the selected good quality waveforms show the characteristic of splitting with clear energy on the radial and transverse component. We started data analysis by determining station pairs over the entire area. We have formed the station pair by selecting the same earthquake event recorded at both (reference and target) stations. Earlier Eken and Tilmann (2014) and Singh et al. (2016) have successfully applied the RST to regional arrays with the interstation distance less than 300 km (e.g., Eken and Tilmann, 2014; Singh et al., 2016). By taking 300 km interstation spacing as the limit in a similar fashion, we have formed 22816 station pairs with four horizontal components available at reference and target stations out of 35649 from 161 teleseismic events prior to the application of technique. To minimise the effects of the coda waves and converted phases, we used a 45s time window starting 15s before the theoretical onset of the direct-S waves on the basis of the IASP91 1-D radial earth velocity model of Kennett (1991). It will exclude the undesired effect of crustal S multiples in the thick Tibetan crust.

The approach adopted in the present study avoids the source side anisotropy by minimising the misfit function between the corrected seismic waveforms at the reference and target stations. At the first stage, an inverse splitting operator depending on a backward angular rotation with two horizontal components, a time shift and the reversal of the back angular rotation is employed to correct the reference station for known receiver-side anisotropy (generally inferred from SKS splitting analyses) when estimating the direct S-derived individual splitting parameter (Eken and Tilmann, 2014). Following the correction of the reference station, S-signals are corrected for splitting parameters (ϕ and δt) in a grid search manner at the target stations. Corrected S-wave signals at reference and target stations are compared to each other for each pair of splitting parameters. Such comparison also allows for time shifts and amplitude corrections to account for the lateral heterogeneities and differences in site response between these stations by optimising the time shift (Δt) and amplitude factor (a). First, we have assigned

splitting parameters that minimised the misfit function simply representing the difference between corrected reference and target station traces as optimum splitting parameters (FPD and TD) for the receiver-side beneath the target station at a given station-pair. Later, taking average of all optimum splitting parameters estimated at station pairs related to a given target station were considered representative for a given event. In the end, station-pair averaged splitting parameters were averaged over all events to estimate final splitting parameters at that given target station.

The RST relies on two most important underlying assumptions: i) the ray path at two stations can be considered equivalent in deeper mantle part and near the source-side region due to the fact that the distance between receiver and target stations is small ($<$ 300km) compared to the epicentral distance , ii) waveform differences between the receiver and target stations are only due to difference in anisotropic structure after correcting any waveform differences in time and amplitude presumably due to the lateral heterogeneities and differences in site response between these stations. Any potential difference between the thickness of the crust and sedimentary layers will also cause the timing and amplitude of converted phase but Eken and Tilmann (2014) earlier showed numerically its influence on expected splitting parameters would be negligible. During the application of the technique, we let ϕ and δt vary from 0 to 180° with an increment of 1° and 0 to 3 s with an increment of 0.05s, respectively. We performed the inverse F-test error analysis of Silver and Chan (1991) for uncertainty estimates of obtained splitting parameters. In this process, we checked the reliability of the individual splitting parameters by comparing variation in the residual energy distribution away from the minimum with the variation according to the preset confidence level of 95%. Here at this stage, the number of degrees of freedom in the data and unknown model parameters become crucial. According to Silver and Chan (1991) one degree of freedom is set to 1s and considering two horizontal components, then the number of degrees of freedom becomes two times the data length, which could be considered as typical value for teleseismic data. In our case, however, the number of unknown model parameters four at the minimum point (FPD, TD, isotropic delay, amplitude correction factor) or two at any given splitting parameters tried in grid search makes the number of degrees of freedom reduced by four or two, respectively. Estimating number of degrees of freedom is a challenging task. For an appropriate uncertainty analysis the band-limited Gaussian noise is required to be justified as reported by Walsh et al. (2013). Thus taking a fixed value for the degrees of freedom as performed in this study will allow us to compare the reliability between different individual splitting estimates rather than absolute value of the error bounds.

An example of the basic steps of the RST can be found in Figure 3 for target stations ES01 and ES35 respectively. Figure 4 present the examples of the obtained splitting parameters at target stations ES19 and ES33, where null or no measurements are reported by Sol et al. (2007). Null splitting may arise possibly due to three reasons: i) if the incoming polarisation direction below an anisotropic layer parallel to the fast or slow axis; ii) if the region looks isotropic in nature due to complex anisotropy (e.g., Saltzer et al., 2000; Wüstefeld and Bokelmann, 2007) iii) region itself is isotropic in nature. Following Eken and Tilmann (2014) and Singh et al. (2016) we also benefited from the F-test with the null-split rejection criteria to be able to avoid the contamination of null measurement with the good splitting measurements. In this process, we theoretically calculated the residual energy under the assumption of null measurements and compare this with the observed residual energy at the minimum. Figure 5 shows two examples of the null splitting measurements at target stations ES29 and ES37 respectively. To ensure the stability of the results we have performed a stepwise quality assessment criterion before calculating the average

splitting parameters at each station. To achieve this aim we consider only those waveform pairs that have (i) normalized residual energy (ΔE) smaller than 0.5; (ii) amplitude correction factor parameter (a) in between 0.4 and 0.6; and (iii) 95% confidence level for null splitting rejection. The waveform pairs that have an FPD error greater than 25° and delay time error greater than half of the delay time itself were rejected. After these quality assessments, we have left with only 3231 waveform pairs. At this stage of the processing, we have performed another visual inspection to enhance the quality of our estimates that finally allowed only very high quality 501 waveform pairs. These final waveforms manifest clear splitting and are free from any distortions due to signal processing. Remaining 501 waveform pairs were extracted from only 25 teleseismic events (Figure 6) and used to calculate the average splitting parameter at each station. The list of these 25 teleseismic events is provided in Table 1. We applied theVon Mises approach (Cochran et al., 2003) to calculate the circular mean at each target stations for ϕ and an arithmetic mean is used for δt.

3.1 RESULTS

We present here 501 splitting measurements observed for 42 seismic stations of the XE network between the years 2003 and 2004. The angular average of individual direct S-derived splitting parameters (ϕ_s and δt_s) at each station is given in Table 2. Station-averaged splitting parameters usually reflect significant anisotropy with large delay times ($>$1 s, Figure 7 and 8) compared to those that could be considered negligible based on early SKS-derived anisotropy parameters. For example at station ES31 direct-S waves provide relatively large time delay (1.23 s) although SKS splitting analysis performed by Sol et al. (2007) earlier resulted in a much smaller time delay of about 0.3 s. We have observed a considerable variation in direct S-waves derived delay times ranging from 0.64 s to 1.68 s. In general, we have observed the SW-NE to W-E trend in ϕ_s before the edge margin of the southeastern Tibetan region. A consistent change in variation of ϕ_s is observed further east where orientations take a sharp change from SSW-ENE or W-E to NW-SE direction (Figure 7). We found significant anisotropy ($\geq$0.64 s) at seismic stations ES19, ES20, ES22, ES32, ES33, ES34, ES42 and ES45, where previously hitherto null or negligible anisotropy obtained with the splitting of SKS waves (Sol et al., 2007). This could stem from multi-layered anisotropic orientations or insufficient amount of SKS-derived splitting measurements. This consideration is inconsistent with isotropic nature of the Indian lithosphere and signifies complex 3D nature of more complex deformation pattern of the EHS. The scatter plot in Figure 8 exhibits a comparison between estimated splitting parameters (ϕ_s and δt_s) from the analysis of direct-S wave and previous SKS splitting measurements (Sol et al., 2007). The observed FPDs and GPS velocity vectors follow nearly the similar trend. The overall variation pattern of S-derived FPDs (ϕ_s) is consistent with the previous SKS measurement. However we observe the larger time delays for the S wave compared to those inferred from SKS phase.

We combined our splitting measurements with existing geodetic measurements (GPS velocity vector, APM velocity vector). The GPS velocities are based on previously published data of Chen et al. (2000); Zhang et al. (2004); Shen et al. (2005); Sol et al. (2007). The APM velocities are calculated via a web-based plate motion calculator (https://www.unavco.org/software/geodetic-utilities/plate-motion-calculator/plate-motion-calculator.html) that is based on an integrated global plate motion model (GSRMv1.2) originally developed by Kreemer et al. (2003). Figure 9 presents a comparison among direct S-derived splitting parameters, APM directions, and GPS measurements in our target region. It suggests that the observed anisotropy is not only due to litho-

spheric deformation or due to asthenospheric dynamics at the base of the lithosphere, but rather implies a combined effect of both.

3.2 DISCUSSION

3.3 Origin of anisotropy in the southeastern Tibetan region

Our resultant splitting measurements that vary in a range of δt_s from 0.64 to 1.68s suggest the presence of significant deformation pattern in the region. The fast polarisation directions are rather consistent and match well with the surface geology, similar to those observed from the SKS phases in Sol et al. (2007). The fast directions closely follow the strike of the major sutures like BNSZ and ITSZ and surface strain fields as observed through GPS and are under the influence of bending at the EHS (Figure 7). Seismic anisotropy directions that are parallel to the surface geologic features such as faults etc. (e.g., Savage, 1999; Flesch et al., 2005) are indicative of vertically coherent deformation of the crust and upper mantle that has been earlier invoked as a possibility to explain the anisotropic character in the eastern and northeastern Tibet (Holt et al., 2000; León Soto et al., 2012; Eken et al., 2013; Eken and Tilmann, 2014). In the absence of any compelling evidence for crust-mantle coupling, we argue in favour of a large-scale deformation of crust and upper mantle under similar boundary conditions as a plausible option to explain the observed anisotropy (Flesch et al., 2005; Sol et al., 2007; Holt et al., 2000).

Observed large time delays (>1s), in this study, reflect a highly anisotropic region with similar deformation patterns at depths. The presence of a more complex anisotropic structure (e.g. double-layer) with different orientation in fast axis at various depths may result in smaller delay times (Saltzer et al., 2000). In the western Himalayan region, Vinnik et al. (2007) observed different fast velocity directions for seismic azimuthal anisotropy that vary from N60°E at depths between 80 and 160 km to N150°E at depths between 160 and 220 km depth by using the joint inversion of the SKS particle motion and P receiver functions. This provides an argument to explain the null or negligible anisotropy as reported from the same region using SKS phases (Sandvol et al., 1994). Smaller time delays in Nepal Himalaya and Sikkim Himalaya were attributed to the combined effect of shear at the base of lithosphere due to APM related strain of Indian plate and ductile flow along the collision front due to compression, with possibly completely different orientations (Singh et al., 2007). Sol et al. (2007) reported the null measurements at few stations without any specif reason. The transition between deformation types at the boundaries of Indian and Eurasian lithospheric plates was considered to be the main reason for observed null or negligible anisotropy further west beneath southern Tibetan Plateau (Chen et al., 2010; Chen and Ozalaybey, 1998; Barruol and Hoffmann, 1999; Zhao et al., 2014). The lack of anisotropy beneath southern Tibet was mainly explained by the isotropic nature of Indian tectonic plate or lack in an ability of SKS phases to sample the anisotropy due to sub-vertical mantle shear strain field created due to downwelling Indian lithosphere (Singh et al., 2007; Sandvol et al., 1997). However the isotropic nature of Indian lithosphere was contradicted in various studies (Singh et al., 2006, 2007; Kumar and Singh, 2008) and significant anisotropy is reported beneath Tibet in the region of null measurement (Gao and Liu, 2009; Singh et al., 2016). Indian lithosphere is considered to be more isotropic in nature to explain the null or negligible anisotropy beneath southern Tibet (Chen and Ozalaybey, 1998; Barruol and Hoffmann, 1999; Chen et al., 2010). Using the same argument to explain the null measurements in our study region

requires the northern extent of the Indian lithospheric mantle beyond of ITSZ. Recent tomographic studies (Griot et al., 1998; Huang et al., 2003; Zhou and Murphy, 2005; Yao et al., 2008; Priestley et al., 2006; Singh et al., 2014; Pandey et al., 2014) suggest that in the western Tibetan side, where the N-S extension is less, the Indian lithosphere is supposed to be up to the Jinsa River Suture Zone (JRSZ) (Zhao et al., 2010), while in the eastern Tibet side the Indian lithosphere is extending up to the ITSZ (Li et al., 2008; Zhao et al., 2010). A combined study using seismic anisotropy and Bouguer gravity anomalies place the Indian mantle front up-to 33°N in central Tibet (Chen et al., 2010). In the segment of the Himalaya-Tibet collision zone, the northern limit of the Indian lithospheric mantle does not seem to extend beyond ITSZ (Li et al., 2008). The lack of anisotropy reported using SKS/SKKS phases (Sol et al., 2007) at a few seismic stations might be due to insufficient measurements. By adding a considerably large amount of measurements from direct-S waves, we have observed significant anisotropy for the same stations and fast axis deformation can be explained by eastward flow in a lithospheric crush zone formed due to collision of Indian and Asian tectonic plates as suggested for southern Tibet (Zhao et al., 2014).

The crust beneath Tibet is thick ($\sim$ 80 km, e.g., Singh et al. (2015)) and crustal anisotropic effects should account in the splitting measurements obtained using direct-S and SKS/SKKS phases. In the Himalayan region highly anisotropic crust ($\sim$20%) has been reported using inversion of receiver functions (Schulte-Pelkum et al., 2005; Singh et al., 2010), while similar approach at few seismic stations covering Tibet suggests for 4-14% seismic anisotropy within the Tibetan crust (Sherrington et al., 2004; Ozacar and Zandt, 2004). Ozacar and Zandt (2004) have accounted for splitting of $<$0.5 s over SKS split times due to the observed anisotropy of $>$ 10% in the crust. Splitting time of 0.2-0.3 s is observed within the eastern Tibet crust using splitting of Moho converted Ps phases (receiver functions) (Chen et al., 2013). Tomographic (Huang et al., 2002, 2009; Hung et al., 2010; Yao et al., 2008, 2010; Li et al., 2009), magnetotelluric (Bai et al., 2010) and gravity (Jordan and Watts, 2005) studies of the SE Tibetan region suggest ductile flow in the deeper region of the crust. Relatively low seismic velocities resolved for the shear waves in the tomographic studies at these crustal depths imply the localized flow of the crustal material along strike slip fault network in the region (Yao et al., 2010). These types of flow may produce splitting orientations similar to lower lithospheric scales with coherent deformation. A coupled crust and mantle increases the SKS delay times by 0.2-0.5 s due to the effects of crust. The anisotropic orientations observed in most parts of Tibet (Sherrington et al., 2004; Ozacar and Zandt, 2004; Chen et al., 2013) within the crust are completely different than the SKS or direct-S waves implying the types of deformation in the crust and upper mantle could be different and does not indicate a coherent deformation at least in parts of Tibet. The most possible explanation for such decoupling could be that the crustal anisotropic parameters are influenced by either current deformation or fossilised fabric with different boundary conditions at mid-crustal and lower crustal levels.

3.4 Comparison between direct S and SKS derived splitting parameters

The scatter plot in Figure 8 (a,b) exhibits a comparison between estimated splitting parameters (ϕ_s and δt_s) from the analysis of direct-S wave and previous SKS splitting measurements (Sol et al., 2007). The obtained splitting parameters (ϕ_s) from the direct-S wave measurements depict that it is consistent with the previous SKS measurements. Overall consistency between splitting parameters inferred from SKS and direct-S waves is most likely because both are exposed to the same type of large-scale anisotropic structures. Large differences between SKS- and S-derived δt_s that appear as a move-out in the scatter plot

occurs due to two reasons: i) longer S-wave ray paths as compared to SKS-wave that is being exposed by the same type of large-scale anisotropy and, ii) an increase in the number of the events (Figure 8c,d) sampling different azimuths that contribute to the direct-S wave measurements as compared to the SKS. The accuracy of results that is evident from small deviations in Figs. 8c,d is most likely due to the involvement of relatively enhanced observations from both S- and SKS phase in splitting measurements. Fig. 8c depict that the absolute deviation for ϕ_s is no longer larger than 25° except stations ES23, ES27, ES31, ES39, ES40, ES41 and ES46, where we observe large deviations up to 48°. We obtained an extreme case of maximum deviation for δt_s at station ES31. The deviation for ϕ_s is also relatively large (>30°). One possible explanation for such large mismatch despite the fact that station ES31 does not suffer from any limited amount of data problem (8 observations for SKS and 14 for S) might be the use of incorrect reference anisotropy knowledge when correcting for receiver-side anisotropy. Overall deviations for δt_s are smaller than 0.56s. In general, we observe relatively more events for the direct S-waves compared to individual SKS phase except at stations ES16, ES18, ES23, ES26 and ES27. For these five stations, we detected deviations for ϕ_s and δt_s up to 36° and 0.5 s, respectively. Summing up, a comparative analysis on splitting parameters shows a good accordance between SKS- and direct S-derived splitting parameters as previously observed in the Himalaya- Tibet collision zone (e.g., McNamara et al., 1994; Singh et al., 2016; Huang et al., 2011; Eken et al., 2013) and in the Indian shield (Saikia et al., 2010).

3.5 Deformation pattern revealed from the comparison of the GPS, APM and splitting measurements

Previous studies on seismic anisotropy (McNamara et al., 1994; Sol et al., 2007; Huang et al., 2000, 2007; Wang et al., 2007, 2008; Chen et al., 2013; Zhao et al., 2014; Guilbert et al., 1996; Bai et al., 2009) that compared splitting parameters with those of APM, GPS and structural and topographical features provide crucial information concerning the dynamic deformation pattern and possible link of the strength of the coupling in between the crust and lithospheric mantle beneath the southeastern or eastern Tibetan region. We have observed a sharp transition in the spatial distribution of ϕ_s from nearly W-E direction to nearly NW-SE or NNW-SSE near the edge margin of the southeastern Tibet. The structural and topographical features, such as major suture zones, mountain belts, etc. tend to rotate around the EHS from nearly E-W or ENE-WSW to N-S or NE-SW direction (Hallet and Molnar, 2001; Booth et al., 2004). The observed FPDs and GPS velocity vectors follow almost similar trend. The absolute plate motion (APM) directions are well consistent with the present ongoing asthenospheric flow (Vinnik et al., 1992, 1995; Vinnik and Montagner, 1996). Results from the comparison between lateral variation of plate motion (APM of Eurasian and Indian plate referenced to NNR frame or relative plate motion of Indian Plate referenced to Eurasian plate) and splitting parameters of this study (Fig. 9) did not indicate any correlation. The discrepancy between the FPD and APM may imply that the obtained splitting and hence the anisotropic behaviour of the study area is not only due to asthenospheric dynamics, but it is a combined effect of the lithospheric deformation and asthenospheric dynamics. The lateral variation of obtained splitting measurements, when taken together with GPS velocity vectors, geological features and the APM directions depict the movement of lithospheric or crustal material of the western and central plateau relative to the Eurasian plate towards the eastern Tibetan side and clockwise rotation around the EHS. This supports presence of a deep crustal flow and movement of materials from the central and western portion towards the eastern Tibetan side that have been earlier suggested by Royden et al. (1997, 2008).

The present day GPS measurements do not reveal the deformation of the whole crust but could be rather associated with the deformation of the shallow crust (Chen et al., 2013). Seismic imaging of the crustal anisotropy based on former receiver function studies (e.g., Sherrington et al., 2004; Chen et al., 2013) also support this argument. The orientation of the GPS velocity and the FPDs of the direct-S waves match only when the orientation of the different layers of anisotropy within the crust and mantle tend to be similar. Griot et al. (1998); Holt et al. (2000); Fouch et al. (2000); Sol et al. (2007) discuss the coupling and decoupling of the crust and mantle by making comparisons among the FPD, GPS, APM and surficial features. Sol et al. (2007) have reported a good coherency between anisotropic and geodetic measurements for the entire southeastern Tibetan region, and on that basis, they discuss the coupling of the crustal and mantle material as similarly observed in the northeast Tibetan Plateau (e.g., Eken et al., 2013; Eken and Tilmann, 2014). The seismic anisotropy directions that were previously obtained from the inversion of receiver functions, however, do not suggest vertically coherent deformation of the crust (e.g., Ozacar and Zandt, 2004; Sherrington et al., 2004). Sherrington et al. (2004) have reported 4–14% seismic anisotropy with different orientations at different depths. They attribute varying pattern of anisotropic directions to both fossilised fabric and more recent deformation. The different orientations at mid and lower crustal levels does not necessarily support a coherent deformation of the crust and upper mantle.

On the basis of driving forces, two kinematic models have been proposed to explain the coupling-decoupling of the crust and lithospheric mantle. First one is a simple asthenospheric model (Richardson, 1992), proposed to explain the decoupling of the crust and mantle by the intrusion of weak mechanical layer such as asthenosphere into the crust. Whenever a weak mechanical layer is present in between the crust and mantle the force acted on the crustal region cannot be transmitted into the mantle. As a result, the crust is decoupled from the mantle due to different driving forces on them. In such models, the velocity difference between the top and bottom of the weak mechanical layer gives rise to the mantle deformation, and that difference is parallel to the fast polarisation direction. The second model proposed by Lithgow-Bertelloni and Richards (1998) is the vertically coherent model, and it explains the coupling of the materials within the crust and lithospheric mantle on the basis of transmission of the buoyancy forces from crust to the mantle. This model requires a rigid lower part of the crust. In contrast, low shear wave velocity anomalies resolved in various tomographic studies recently (Huang et al., 2002, 2009; Hung et al., 2010; Yao et al., 2008; Li et al., 2009) have indicated a weak layer in the deeper region of the crust beneath the SE Tibetan region. It is noteworthy to mention that we avoid making any comment on the possible linkage between deformation and coupling of crust and underlying lithospheric mantle by only using splitting parameters inferred from direct-S waves and geodetic measurements and further studies are required.

4 Conclusions

Our splitting observations using direct-S waves add new constraints in understanding the deformation patterns and their causes in the southeastern Tibetan region near Namche Barwa. We list the main concluding remarks from the present study as follows:

1. The observed splitting parameters suggest for a highly deformed crust and lithospheric mantle.

2. Significant anisotropy is observed at seismic stations where null or no measurements are reported based on earlier SKS splitting measurements.

3. Our study also provides clear evidence for the development of anisotropy in the region with active geodynamic implications of several tectonic events, i.e., the multistage subduction of Indian plate below the Eurasian plate, the movement of the western central Tibetan lithospheric material towards the southeastern and eastern Tibetan side and slab-rollback towards Burma.

4. The observed anisotropic delays (0.67-1.68) suggest the possible existence of a multi-layered anisotropy structure in the crust and upper mantle. Further understanding this requires 3-D geodynamic modelling and inversion of multi-frequency datasets to resolve more complex depth-dependent anisotropic structures (e.g. multi-layer anisotropy, dipping axis of symmetry).

5 Code availability

The multisplit C++ code used for carrying out splitting measurements of the direct S waveforms is available with a General Public License (GPL) license at http://github.com/ftilmann/multisplit.

6 Data availability

The waveform data used in this study are downloaded from the Incorporated Research Institutions for Seismology Data Management Center (IRIS-DMC) data archive system Namche Barwa Tibet network code XE (2003-2004).

Acknowledgements. The IRIS data management centre and Project team of Namche Barwa Seismic Network (PASSCAL) are gratefully acknowledged for making the seismic data available. This work has been performed under the ISIRD project (ASI) of IIT Kharagpur. T. Eken appreciates Alexander von Humboldt (AvH) Foundation for the equipment subsidy. We benefited from valuable comments by Frederik Tilmann during the preparation of revised version of the paper. We thank Topical Editor Charlotte Krawczyk, reviewer Rob Porritt and one anonymous reviewer for their valuable comments and suggestions which helped us to improve the manuscript substantially.

References

Argand, E.: La tectonique de l'Asie, Int. geol, Congr. Rep, pp. 171–322, 1924.

Bai, D., Unsworth, M. J., Meju, M. A., Ma, X., Teng, J., Kong, X., Sun, Y., Sun, J., Wang, L., Jiang, C., et al.: Crustal deformation of the eastern Tibetan plateau revealed by magnetotelluric imaging, Nature geoscience, 3, 358–362, doi:10.1038/ngeo830, 2010.

Bai, L., Iidaka, T., Kawakatsu, H., Morita, Y., and Dzung, N.: Seismic anisotropy and shear-wave splitting in lower-crustal and upper-mantle rocks from the Ivrea Zone—experimental and calculated data, Phys. Earth Planet. Inter., 176, 33–43, doi:10.1016/j.pepi.2009.03.008, 2009.

Barruol, G. and Hoffmann, R.: Upper mantle anisotropy beneath the Geoscope stations, J. Geophys. Res., 104, 10 757–10 773, doi:10.1029/1999JB900033, 1999.

Becker, T. W. and Faccenna, C.: Mantle conveyor beneath the Tethyan collisional belt, Earth Planet. Sci. Lett., 310, 453 – 461, doi:10.1016/j.epsl.2011.08.021, 2011.

Booth, A. L., Zeitler, P. K., Kidd, W. S., Wooden, J., Liu, Y., Idleman, B., Hren, M., and Chamberlain, C. P.: U-Pb zircon constraints on the tectonic evolution of southeastern Tibet, Namche Barwa Area, American Journal of Science, 304, 889–929, doi:10.2475/ajs.304.10.889, 2004.

Chen, W.-P. and Ozalaybey, S.: Correlation between seismic anisotropy and Bouguer gravity anomalies in Tibet and its implications for lithospheric structures, Geophys. J. Int., 135, 93–101, doi:10.1046/j.1365-246X.1998.00611.x, 1998.

Chen, W.-P., Martin, M., Tseng, T.-L., Nowack, R. L., Hung, S.-H., and Huang, B.-S.: Shear-wave birefringence and current configuration of converging lithosphere under Tibet, Earth Planet. Sci. Lett., 295, 297 – 304, doi:10.1016/j.epsl.2010.04.017, 2010.

Chen, Y., Zhang, Z., Sun, C., and Badal, J.: Crustal anisotropy from Moho converted Ps wave splitting analysis and geodynamic implications beneath the eastern margin of Tibet and surrounding regions, Geophys. Res. Lett., 24, 946–957, doi:10.1016/j.gr.2012.04.003, 2013.

Chen, Z., Burchfiel, B., Liu, Y., King, R., Royden, L., Tang, W., Wang, E., Zhao, J., and Zhang, X.: Global Positioning System measurements from eastern Tibet and their implications for India/Eurasia intercontinental deformation, J. Geophys. Res., 105, 16 215–16 227, doi:10.1029/2000JB900092, 2000.

Cochran, E. S., Vidale, J. E., and Li, Y.-G.: Near-fault anisotropy following the Hector Mine earthquake, JGR, 108, n/a–n/a, doi:10.1029/2002JB002352, 2003.

Confal, J. M., Eken, T., Tilmann, F., Yolsal-Çevikbilen, S., Çubuk-Sabuncu, Y., Saygin, E., and Taymaz, T.: Investigation of mantle kinematics beneath the Hellenic-subduction zone with teleseismic direct shear waves, Phys. Earth Planet. Inter., 261, 141–151, doi:10.1016/j.pepi.2016.10.012, 2016.

Eken, T. and Tilmann, F.: The Use of Direct Shear Waves in Quantifying Seismic Anisotropy: Exploiting Regional Arrays, Bull. Seismol. Soc. Am., 104, 2644–2661, doi:10.1785/0120140020, 2014.

Eken, T., Tilmann, F., Mechie, J., Zhao, W., Kind, R., Su, H., Xue, G., and Karplus, M.: Seismic Anisotropy from SKS Splitting beneath Northeastern Tibet, Bull. Seismol. Soc. Am., 103, 3362–3371, doi:10.1785/0120130054, 2013.

Flesch, L. M., Haines, A. J., and Holt, W. E.: Dynamics of the India-Eurasia collision zone, J. Geophys. Res., 106, 16 435–16 460, doi:10.1029/2001JB000208, 2001.

Flesch, L. M., Holt, W. E., Silver, P. G., Stephenson, M., Wang, C.-Y., and Chan, W. W.: Constraining the extent of crust–mantle coupling in central Asia using GPS, geologic, and shear wave splitting data, Earth Planet. Sci. Lett., 238, 248 – 268, doi:10.1016/j.epsl.2005.06.023, 2005.

Fouch, M. J., Fischer, K. M., Parmentier, E. M., Wysession, M. E., and J., C. T.: Shear wave splitting, continental keels, and patterns of mantle flow, J. Geophys. Res., 105, 6255–6275, doi:10.1029/1999JB900372, 2000.

Fu, Y. V., Chen, Y. J., Li, A., Zhou, S., Liang, X., Ye, G., Jin, G., Jiang, M., and Ning, J.: Indian mantle corner flow at southern Tibet revealed by shear wave splitting measurements, Geophys. Res. Lett., 35, n/a–n/a, doi:10.1029/2007GL031753, 2008.

Gao, S. S. and Liu, K. H.: Significant seismic anisotropy beneath the southern Lhasa Terrane, Tibetan Plateau, Geochem., Geophys., Geosys., 10, n/a–n/a, doi:10.1029/2008GC002227, 2009.

Garzanti, E. and Van Haver, T.: The Indus clastics: forearc basin sedimentation in the Ladakh Himalaya (India), SG, 59, 237–249, doi:10.1016/0037-0738(88)90078-4, 1988.

Griot, D.-A., Montagner, J.-P., and Tapponnier, P.: Phase velocity structure from Rayleigh and Love waves in Tibet and its neighboring regions, J. Geophys. Res., 103, 21 215–21 232, doi:10.1029/98JB00953, 1998.

Guilbert, J., Poupinet, G., and Mei, J.: A study of azimuthal P residuals and shear-wave splitting across the Kunlun range (Northern Tibetan plateau), Phys. Earth Planet. Inter., 95, 167–174, doi:10.1016/0031-9201(95)03120-0, 1996.

Hallet, B. and Molnar, P.: Distorted drainage basins as markers of crustal strain east of the Himalaya, J. Geophys. Res., 106, 13 697–13 709, doi:10.1029/2000JB900335, 2001.

Henderson, A. L., Najman, Y., Parrish, R., Mark, D. F., and Foster, G. L.: Constraints to the timing of India–Eurasia collision; a re-evaluation of evidence from the Indus Basin sedimentary rocks of the Indus–Tsangpo Suture Zone, Ladakh, India, Earth-Sci. Rev., 106, 265–292, doi:10.1016/j.earscirev.2011.02.006, 2011.

Herquel, G., Wittlinger, G., and Guilbert, J.: Anisotropy and crustal thickness of northern-Tibet. New constraints for tectonic modelling, Geophys. Res. Lett., 22, 1925–1928, doi:10.1029/95GL01789, 1995.

Hirn, A., Jiang, M., Sapin, M., Diaz, J., Nercessian, A., and Lu, Q.: Seismic anisotropy as an indicator of mantle flow beneath the Himalayas and Tibet, Nature, 375, 571–574, doi:10.1038/375571a0, 1995.

Holt, W., Chamot-Rooke, N., Le Pichon, X., Haines, A., Shen-Tu, B., and Ren, J.: Velocity field in Asia inferred from Quaternary fault slip rates and Global Positioning System observations, J. Geophys. Res., 105, 19 185–19 209, doi:10.1029/2000JB900045, 2000.

Holt, W. E., Li, M., and Haines, A.: Earthquake strain rates and instantaneous relative motions within central and eastern Asia, Geophys. J. Int., 122, 569–593, doi:10.1111/j.1365-246X.1995.tb07014.x, 1995.

Houseman, G. and England, P.: Finite strain calculations of continental deformation: 1. Method and general results for convergent zones, J. Geophys. Res., 91, 3651–3663, doi:10.1029/JB091iB03p03651, 1986.

Houseman, G. and England, P.: Crustal thickening versus lateral expulsion in the Indian-Asian continental collision, J. Geophys. Res., 98, 12 233–12 249, doi:10.1029/93JB00443, 1993.

Houseman, G. and England, P.: A lithospheric-thickening model for the Indo-Asian collision, WORLD AND REGIONAL GEOLOGY, 1, 1–17, 1996.

Huang, J., Zhao, D., and Zheng, S.: Lithospheric structure and its relationship to seismic and volcanic activity in southwest China, J. Geophys. Res., 107, ESE 13–1–ESE 13–14, doi:10.1029/2000JB000137, 2002.

Huang, W.-C., Ni, J. F., Tilmann, F., Nelson, D., Guo, J., Zhao, W., Mechie, J., Kind, R., Saul, J., Rapine, R., and Hearn, T. M.: Seismic polarization anisotropy beneath the central Tibetan Plateau, J. Geophys. Res., 105, 27 979–27 989, doi:10.1029/2000JB900339, 2000.

Huang, Z., Wang, L., Xu, M., Liu, J., Mi, N., and Liu, S.: Shear wave splitting across the Ailao Shan-Red River fault zone, SW China, Geophys. Res. Lett., 34, n/a–n/a, doi:10.1029/2007GL031236, 2007.

Huang, Z., Li, H., Zheng, Y., and Peng, Y.: The lithosphere of North China Craton from surface wave tomography, Earth Planet. Sci. Lett., 288, 164–173, doi:10.1016/j.epsl.2009.09.019, 2009.

Huang, Z., Wang, L., Zhao, D., Mi, N., and Xu, M.: Seismic anisotropy and mantle dynamics beneath China, Earth Planet. Sci. Lett., 306, 105 – 117, doi:10.1016/j.epsl.2011.03.038, 2011.

Huang, Z.-M., Zhang, Y.-Z., Kotaki, M., and Ramakrishna, S.: A review on polymer nanofibers by electrospinning and their applications in nanocomposites, Composites science and technology, 63, 2223–2253, doi:10.1016/S0266-3538(03)00178-7, 2003.

Hung, S.-H., Chen, W.-P., Chiao, L.-Y., and Tseng, T.-L.: First multi-scale, finite-frequency tomography illuminates 3-D anatomy of the Tibetan plateau, Geophys. Res. Lett., 37, n/a–n/a, doi:10.1029/2009GL041875, 2010.

Jagoutz, O., Royden, L., Holt, A. F., and Becker, T. W.: Anomalously fast convergence of India and Eurasia caused by double subduction, Nature Geoscience, 8, 475–478, doi:10.1038/ngeo2418, 2015.

Jordan, T. and Watts, A.: Gravity anomalies, flexure and the elastic thickness structure of the India–Eurasia collisional system, Earth Planet. Sci. Lett., 236, 732–750, doi:10.1016/j.epsl.2005.05.036, 2005.

Karato, S.-I.: Grain-size distribution and rheology of the upper mantle, Tectonophys, 104, 155–176, doi:1016/0040-1951(84)90108-2, 1984.

Karato, S.-I.: Seismic anisotropy due to lattice preferred orientation of minerals: Kinematic or dynamic?, Geophysical Monograph Series., 39, 455–471, doi:10.1029/GM039p0455, 1987.

Karato, S.-i. and Wu, P.: Rheology of the Upper Mantle: A Synthesis, Science, 260, 771–778, doi:10.1126/science.260.5109.771, 1993.

Karplus, M., Zhao, W., Klemperer, S., Wu, Z., Mechie, J., Shi, D., Brown, L., and Chen, C.: Injection of Tibetan crust beneath the south Qaidam Basin: Evidence from INDEPTH IV wide-angle seismic data, J. Geophys. Res., 116, n/a–n/a, doi:10.1029/2010JB007911, 2011.

Kennett, B. L. N.and Engdahl, E.: Traveltimes for global earthquake location and phase identification, Geophys. J. Int., 105, 429–465, doi:10.1111/j.1365-246X.1991.tb06724.x, 1991.

Kreemer, C., Holt, W. E., and Haines, A. J.: An integrated global model of present-day plate motions and plate boundary deformation, Geophys. J. Int., 154, 8–34, doi:10.1046/j.1365-246X.2003.01917.x, 2003.

Kumar, M. R. and Singh, A.: Evidence for plate motion related strain in the Indian shield from shear wave splitting measurements, J. Geophys. Res., 113, n/a–n/a, doi:10.1029/2007JB005128, 2008.

Kumar, P., Yuan, X., Kind, R., and Ni, J.: Imaging the colliding Indian and Asian lithospheric plates beneath Tibet, J. Geophys. Res., 111, n/a–n/a, doi:10.1029/2005JB003930, b06308, 2006.

Lavé, J., Avouac, J., Lacassin, R., Tapponnier, P., and Montagner, J.: Seismic anisotropy beneath Tibet: evidence for eastward extrusion of the Tibetan lithosphere?, EPSL, 140, 83–96, doi:10.1016/0012-821X(96)00045-3, 1996.

León Soto, G., Sandvol, E., Ni, J. F., Flesch, L., Hearn, T. M., Tilmann, F., Chen, J., and Brown, L. D.: Significant and vertically coherent seismic anisotropy beneath eastern Tibet, J. Geophys. Res., 117, n/a–n/a, doi:10.1029/2011JB008919, 2012.

Lev, E., Long, M. D., and van der Hilst, R. D.: Seismic anisotropy in Eastern Tibet from shear wave splitting reveals changes in lithospheric deformation, EPSL, 251, 293–304, doi:10.1016/j.epsl.2006.09.018, 2006.

Li, C., Van der Hilst, R. D., Meltzer, A. S., and Engdahl, E. R.: Subduction of the Indian lithosphere beneath the Tibetan Plateau and Burma, EPSL, 274, 157–168, doi:10.1016/j.epsl.2008.07.016, 2008.

Li, Y. H., Wu, Q. J., and Tian, X. B.: Crustal structure in the Yunnan region determined by modeling receiver functions, Chinese J. Geophys., 52, 67–80, 2009.

Lithgow-Bertelloni, C. and Richards, M. A.: The dynamics of Cenozoic and Mesozoic plate motions, Rev. Geophys., 36, 27–78, doi:10.1029/97RG02282, 1998.

Mainprice, D., Barruol, G., and Ismail, W. B.: The seismic anisotropy of the Earth's mantle: from single crystal to polycrystal, Earth's Deep Interior: Mineral physics and tomography from the atomic to the global scale, pp. 237–264, doi:10.1029/GM117p0237, 2000.

McKenzie, D. and Priestley, K.: The influence of lithospheric thickness variations on continental evolution, Lithos, 102, 1–11, doi:10.1016/j.lithos.2007.05.005, 2008.

McNamara, D. E., Owens, T. J., Silver, P. G., and Wu, F. T.: Shear wave anisotropy beneath the Tibetan Plateau, J. Geophys. Res., 99, 13 655–13 665, doi:10.1029/93JB03406, 1994.

Molnar, P. and Tapponnier, P.: Cenozoic tectonics of Asia: effects of a continental collision, Science, 189, 419–426, doi:10.1126/science.189.4201.419, 1975.

Nelson, K. D., Zhao, W., Brown, L., Kuo, J., Che, J., Liu, X., Klemperer, S., Makovsky, Y., Meissner, R., Mechie, J., et al.: Partially molten middle crust beneath southern Tibet: synthesis of project INDEPTH results, Science, 274, 1684–1688, doi:10.1126/science.274.5293.1684, 1996.

Nicolas, A. and Christensen, N. I.: Formation of Anisotropy in Upper Mantle Peridotites-A Review, Composition, structure and dynamics of the lithosphere-asthenosphere system, pp. 111–123, doi:10.1029/GD016p0111, 1987.

Ozacar, A. A. and Zandt, G.: Crustal seismic anisotropy in central Tibet: Implications for deformational style and flow in the crust, Geophys. Res. Lett., 31, n/a–n/a, doi:10.1029/2004GL021096, 2004.

Pandey, S., Yuan, X., Debayle, E., Priestley, K., Kind, R., Tilmann, F., and Li, X.: A 3D shear-wave velocity model of the upper mantle beneath China and the surrounding areas, Tectonophys, 633, 193–210, doi:10.1016/j.tecto.2014.07.011, 2014.

Priestley, K., Debayle, E., McKenzie, D., and Pilidou, S.: Upper mantle structure of eastern Asia from multimode surface waveform tomography, J. Geophys. Res., 111, n/a–n/a, doi:10.1029/2005JB004082, 2006.

Replumaz, A. and Tapponnier, P.: Reconstruction of the deformed collision zone between India and Asia by backward motion of lithospheric blocks, J. Geophys. Res., 108, n/a–n/a, doi:10.1029/2001JB000661, 2003.

Richardson, R.: Ridge forces, absolute plate motions, and the intraplate stress field, J. Geophys. Res., 97, 11 739–11 748, doi:10.1029/91JB00475, 1992.

Rowley, D. B. and Currie, B. S.: Palaeo-altimetry of the late Eocene to Miocene Lunpola basin, central Tibet, Nature, 439, 677–681, doi:10.1038/nature04506, 2006.

Royden, L. H., Burchfiel, B. C., King, R. W., Wang, E., Chen, Z., Shen, F., and Liu, Y.: Surface deformation and lower crustal flow in eastern Tibet, Science, 276, 788–790, doi:10.1126/science.276.5313.788, 1997.

Royden, L. H., Burchfiel, B. C., and van der Hilst, R. D.: The geological evolution of the Tibetan Plateau, Science, 321, 1054–1058, doi:10.1126/science.1155371, 2008.

Saikia, D., Ravi Kumar, M., Singh, A., Mohan, G., and Dattatrayam, R. S.: Seismic anisotropy beneath the Indian continent from splitting of direct S waves, J. Geophys. Res., 115, n/a–n/a, doi:10.1029/2009JB007009, 2010.

Saltzer, R. L., Gaherty, J. B., and Jordan, T. H.: How are vertical shear wave splitting measurements affected by variations in the orientation of azimuthal anisotropy with depth?, Geophys. J. Int., 141, 374–390, doi:10.1046/j.1365-246X.2000.00088.x, 2000.

Sandvol, E., Ni, J., Kind, R., and Zhao, W.: Seismic anisotropy beneath the southern Himalayas-Tibet collision zone, J. Geophys. Res., 102, 17 813–17 823, doi:10.1029/97JB01424, 1997.

Sandvol, E. A., Ni, J. F., Hearn, T. M., and Roecker, S.: Seismic azimuthal anisotropy beneath the Pakistan Himalayas, Geophys. Res. Lett., 21, 1635–1638, doi:10.1029/94GL01386, 1994.

Sato, H., Fehler, M. C., and Maeda, T.: Seismic wave propagation and scattering in the heterogeneous earth, vol. 496, Springer, doi:10.1007/978-3-540-89623-4, 2012.

Savage, M. K.: Seismic anisotropy and mantle deformation: What have we learned from shear wave splitting?, Rev. Geophys., 37, 65–106, doi:10.1029/98RG02075, 1999.

Schulte-Pelkum, V., Monsalve, G., Sheehan, A., Pandey, M. R., Sapkota, S., Bilham, R., and Wu, F.: Imaging the Indian subcontinent beneath the Himalaya, Nature, 435, 1222–1225, doi:10.1038/nature03678, 2005.

Shen, F., Royden, L. H., and Burchfiel, B. C.: Large-scale crustal deformation of the Tibetan Plateau, J. Geophys. Res., 106, 6793–6816, doi:10.1029/2000JB900389, 2001.

Shen, Z.-K., Lü, J., Wang, M., and Bürgmann, R.: Contemporary crustal deformation around the southeast borderland of the Tibetan Plateau, J. Geophys. Res., 110, n/a–n/a, doi:10.1029/2004JB003421, 2005.

Sherrington, H. F., Zandt, G., and Frederiksen, A.: Crustal fabric in the Tibetan Plateau based on waveform inversions for seismic anisotropy parameters, JGR, 109, n/a–n/a, doi:10.1029/2002JB002345, 2004.

Silver, P. G. and Chan, W. W.: Shear wave splitting and subcontinental mantle deformation, JGR, 96, 16 429–16 454, doi:10.1029/91JB00899, 1991.

Singh, A., Kumar, M. R., Raju, P. S., and Ramesh, D. S.: Shear wave anisotropy of the northeast Indian lithosphere, Geophys. Res. Lett., 33, doi:10.1029/2006GL026106, 2006.

Singh, A., Kumar, M. R., and Raju, P. S.: Mantle deformation in Sikkim and adjoining Himalaya: Evidences for a complex flow pattern, Phys. Earth Planet. Inter., 164, 232–241, doi:10.1016/0031-9201(93)90156-4, 2007.

Singh, A., Kumar, M. R., and Raju, P. S.: Seismic structure of the underthrusting Indian crust in Sikkim Himalaya, Tectonics, 29, doi:10.1029/2010TC002722, 2010.

Singh, A., Mercier, J.-P., Ravi Kumar, M., Srinagesh, D., and Chadha, R. K.: Continental scale body wave tomography of India: Evidence for attrition and preservation of lithospheric roots, Geochem., Geophys., Geosys., 15, 658–675, doi:10.1002/2013GC005056, 2014.

Singh, A., Singh, C., and Kennett, B.: A review of crust and upper mantle structure beneath the Indian subcontinent, Tectonophys, 644, 1–21, doi:10.1016/j.tecto.2015.01.007, 2015.

Singh, A., Eken, T., Mohanty, D. D., Saikia, D., Singh, C., and Kumar, M. R.: Significant seismic anisotropy beneath southern Tibet inferred from splitting of direct S-waves, Phys. Earth Planet. Inter., 250, 1–11, doi:10.1016/j.pepi.2015.11.001, 2016.

Sol, S., Meltzer, A., Bürgmann, R., Van der Hilst, R., King, R., Chen, Z., Koons, P., Lev, E., Liu, Y., Zeitler, P., et al.: Geodynamics of the southeastern Tibetan Plateau from seismic anisotropy and geodesy, Geology, 35, 563–566, doi:10.1130/G23408A.1, 2007.

Tapponnier, P., Peltzer, G., Le Dain, A., Armijo, R., and Cobbold, P.: Propagating extrusion tectonics in Asia: New insights from simple experiments with plasticine, Geology, 10, 611–616, doi:10.1130/0091-7613, 1982.

Tapponnier, P., Zhiqin, X., Roger, F., Meyer, B., Arnaud, N., Wittlinger, G., and Jingsui, Y.: Oblique stepwise rise and growth of the Tibet Plateau, Science, 294, 1671–1677, doi:10.1126/science.105978, 2001.

Tseng, T.-L., Chen, W.-P., and Nowack, R. L.: Northward thinning of Tibetan crust revealed by virtual seismic profiles, Geophys. Res. Lett., 36, n/a–n/a, doi:10.1029/2009GL040457, l24304, 2009.

Van Hinsbergen, D. J., Lippert, P. C., Dupont-Nivet, G., McQuarrie, N., Doubrovine, P. V., Spakman, W., and Torsvik, T. H.: Greater India Basin hypothesis and a two-stage Cenozoic collision between India and Asia, Proceedings of the National Academy of Sciences, 109, 7659–7664, doi:10.1073/pnas.1117262109, 2012.

Vinnik, L. and Montagner, J.-P.: Shear wave splitting in the mantle Ps phases, Geophys. Res. Lett., 23, 2449–2452, doi:10.1029/96GL02263, 1996.

Vinnik, L., Green, R., and Nicolaysen, L.: Recent deformations of the deep continental root beneath southern Africa, Nature, 375, 50–52, doi:10.1038/375050a0, 1995.

Vinnik, L., Singh, A., Kiselev, S., and Kumar, M. R.: Upper mantle beneath foothills of the western Himalaya: subducted lithospheric slab or a keel of the Indian shield?, Geophys. J. Int., 171, 1162–1171, doi:10.1111/j.1365-246X.2007.03577.x, 2007.

Vinnik, L. P., Makeyeva, L. I., Milev, A., and Usenko, A. Y.: Global patterns of azimuthal anisotropy and deformations in the continental mantle, Geophys. J. Int., 111, 433–447, doi:10.1111/j.1365-246X.1992.tb02102.x, 1992.

Walsh, B. M., Sibeck, D. G., Nishimura, Y., and Angelopoulos, V.: Statistical analysis of the plasmaspheric plume at the magnetopause, J. Geophys. Res., 118, 4844–4851, doi:10.1002/jgra.50458, 2013.

Wang, C., Chang, L., Lü, Z., Qin, J., Su, W., Silver, P., and Flesch, L.: Seismic anisotropy of upper mantle in eastern Tibetan Plateau and related crust-mantle coupling pattern, Science in China Series D: Earth Sciences, 50, 1150–1160, doi:10.1007/s11430-007-0053-5, 2007.

Wang, C.-Y., Flesch, L. M., Silver, P. G., Chang, L.-J., and Chan, W. W.: Evidence for mechanically coupled lithosphere in central Asia and resulting implications, Geology, 36, 363–366, doi:10.1130/G24450A.1, 2008.

Wüstefeld, A. and Bokelmann, G.: Null detection in shear-wave splitting measurements, Bull. Seismol. Soc. Am., 97, 1204–1211, doi:10.1785/0120060190, 2007.

Wüstefeld, A., Bokelmann, G., Zaroli, C., and Barruol, G.: SplitLab: A shear-wave splitting environment in Matlab, CG, 34, 515–528, doi:10.1016/j.cageo.2007.08.002, 2008.

Yao, H., Beghein, C., and Van Der Hilst, R. D.: Surface wave array tomography in SE Tibet from ambient seismic noise and two-station analysis-II. Crustal and upper-mantle structure, Geophys. J. Int., 173, 205–219, doi:10.1111/j.1365-246X.2007.03696.x, 2008.

Yao, H., Van Der Hilst, R. D., and Montagner, J.-P.: Heterogeneity and anisotropy of the lithosphere of SE Tibet from surface wave array tomography, JGR, 115, n/a–n/a, doi:10.1029/2009JB007142, 2010.

Yin, A. and Harrison, T. M.: Geologic Evolution of the Himalayan-Tibetan Orogen, Annual Rev. Earth Planet Sci., 28, 211 – 280, doi:10.1146/annurev.earth.28.1.211, 2000.

Zhang, P.-Z., Shen, Z., Wang, M., Gan, W., Bürgmann, R., Molnar, P., Wang, Q., Niu, Z., Sun, J., Wu, J., et al.: Continuous deformation of the Tibetan Plateau from global positioning system data, Geology, 32, 809–812, doi:10.1130/G20554.1, 2004.

Zhao, J., Yuan, X., Liu, H., Kumar, P., Pei, S., Kind, R., Zhang, Z., Teng, J., Ding, L., Gao, X., et al.: The boundary between the Indian and Asian tectonic plates below Tibet, Proceedings of the National Academy of Sciences, 107, 11 229–11 233, doi:10.1073/pnas.1001921107, 2010.

Zhao, J., Murodov, D., Huang, Y., Sun, Y., Pei, S., Liu, H., Zhang, H., Fu, Y., Wang, W., Cheng, H., et al.: Upper mantle deformation beneath central-southern Tibet revealed by shear wave splitting measurements, Tectonophys, 627, 135–140, doi:10.1016/j.tecto.2013.11.003, 2014.

Zhou, H. and Murphy, M. A.: Tomographic evidence for wholesale underthrusting of India beneath the entire Tibetan plateau, J. Asian Earth Sci., 25, 445 – 457, doi:10.1016/j.jseaes.2004.04.007, 2005.

Table 1. List of the earthquakes used in this study.

event date	event time	latitude(°)	longitude(°)	depth (m)	magnitude	location site	event id
2003/10/04	14:49:02.7	-07.05	+125.41	532.7	5.5	BANDA SEA	B100403C
2003/10/17	17:19:53.6	-05.08	+102.46	35.1	5.6	SOUTHERN SUMATRA, INDONE	B101703D
2003/11/09	19:23:28.6	+01.56	+127.36	133.9	5.8	HALMAHERA, INDONESIA	B110903E
2004/02/08	08:58:51.8	-03.66	+135.34	25.7	5.7	IRIAN JAYA REGION, INDON	C020804C
2004/02/20	05:58:45.2	-11.61	+166.45	84.0	5.6	SANTA CRUZ ISLANDS	C022004A
2004/03/17	05:21:00.8	+34.59	+023.33	24.5	5.9	CRETE, GREECE	C031704C
2004/03/26	15:20:06.6	+41.86	+144.21	22.4	5.7	HOKKAIDO, JAPAN REGION	C032604D
2004/04/09	15:23:35.0	-13.17	+167.20	228.4	5.8	VANUATU ISLANDS	C040904B
2004/05/28	12:38:44.3	+36.25	+051.62	17.0	6.2	NORTHERN AND CENTRAL IRA	C052804A
2004/06/22	09:04:43.9	-10.90	+166.26	152.8	5.8	SANTA CRUZ ISLANDS	C062204E
2004/06/30	23:37:25.5	+00.80	+124.73	90.8	6.0	MINAHASSA PENINSULA, SUL	C063004F
2004/07/08	10:30:49.2	+47.20	+151.30	128.5	5.9	KURIL ISLANDS	C070804A
2004/07/25	14:35:19.1	-02.43	+103.98	582.1	6.8	SOUTHERN SUMATRA, INDONE	C072504B
2003/07/27	06:25:32.0	+47.15	+139.25	470.3	6.3	PRIMOR'YE, RUSSIA	C072703C
2004/08/02	02:36:54.9	-05.47	+102.62	40.5	5.5	SOUTHERN SUMATRA, INDONE	C080204B
2004/08/07	14:18:35.2	-06.24	+095.67	20.7	5.8	SOUTHWEST OF SUMATRA, IN	C080704D
2004/08/28	17:00:58.2	-08.69	+157.25	10.0	5.5	SOLOMON ISLANDS	C082804F
2003/08/31	23:08:00.3	+43.39	+132.27	481.1	5.5	PRIMOR'YE, RUSSIA	C083103C
2003/09/11	21:58:25.5	-08.20	+156.16	10.0	5.5	SOLOMON ISLANDS	C091103C
2004/09/15	19:10:50.6	+14.22	+120.41	115.4	6.0	LUZON, PHILIPPINES	C091504D
2003/10/11	00:08:49.1	+41.92	+144.36	33.0	5.9	HOKKAIDO, JAPAN REGION	C101103A
2003/10/11	01:11:31.2	+43.97	+148.21	51.2	6.2	EAST OF KURIL ISLANDS	C101103C
2003/10/17	10:19:06.8	-05.47	+154.15	133.0	6.2	SOLOMON ISLANDS	C101703B
2003/10/22	11:45:30.8	-06.06	+147.73	53.5	6.2	EASTERN NEW GUINEA REG.,	C102203C
2003/11/12	08:26:43.7	+33.17	+137.07	384.9	6.1	NEAR S. COAST OF HONSHU,	C111203E

Table 2. Obtained average splitting parameter (ϕ_s and δt_s) estimated from direct-S wave splitting measurement.

stations	latitude(°)	longitude(°)	ϕ_s (°)	δt_s(sec)	number of event at a station	contributing reference stations
ES01	31.26	92.09	73.9	1.5	31	2,3,4,5,7,8,9,10,11,12,36,38,39,40,41
ES02	31.00	92.54	75.7	1.5	26	1,3,4,5,7,8,9,10,11,12,13,38,40,41
ES03	30.75	92.86	81.7	1.2	16	2, 4,5,7,8,10,11,12,38,39,43
ES04	30.65	93.25	91.5	1.2	11	1,3,5,7,8,10,11,12
ES05	31.68	92.40	71.2	1.1	14	1,2,3,4,7,8,10,11,12,13
ES07	31.48	93.70	93.8	1.0	15	1,2,3,4,5,8,9,10,11,12,14,38
ES08	31.28	93.84	106.3	0.9	12	1,2,4,5,7,10,11,12,13
ES09	31.91	93.06	81.5	1.1	15	1,3,5,8,10,11,12,13,14
ES10	31.84	93.79	103.1	1.0	19	1,2,3,4,5,7,8,9,11,12,14,38
ES11	31.91	94.14	96.2	1.2	25	1,2,3,4,5,7,8,9,10,12,14,36,38
ES12	31.59	94.71	101.3	1.2	28	1,2,3,4,5,7,8,9,10,11,13,14,15,23,25,38
ES13	31.54	95.28	88.5	1.4	15	2,4,9,11,12,13,14,15,26,30,36,38
ES14	31.25	95.90	102.9	1.2	24	3,4,7,9,10,11,12,13,15,17,23,25,31
ES15	31.19	96.50	104.2	1.0	09	11,12,14,16,25,36,38
ES16	31.18	97.02	117.0	1.4	01	13
ES17	31.27	97.55	135.4	1.0	11	18,23,25,31
ES18	31.30	97.96	122.0	0.8	02	17
ES19	30.81	95.71	106.6	1.5	09	3,4,7,8,11,12,38
ES20	30.73	96.10	108.0	0.9	01	11
ES22	30.81	96.70	110.0	0.9	01	14
ES23	30.69	97.26	96.2	1.0	16	12,15,25,31
ES24	30.50	97.14	106.0	1.1	03	13, 15
ES25	30.12	97.30	121.1	0.9	10	18,23,31
ES26	29.96	97.51	142.2	1.0	03	14,30,31
ES27	29.64	97.90	130.0	1.1	01	26
ES29	30.01	96.69	84.0	1.1	16	14,15,23,25,31
ES30	29.32	97.19	110.8	1.1	07	25,26,27,31
ES31	29.51	96.76	82.4	1.2	16	14,17,25,26,30,31
ES32	29.76	96.10	103.0	1.4	02	13,30

Table 2. Continued.

stations	latitude(°)	longitude(°)	ϕ_s (°)	δt_s(sec)	number of event at a station	contributing reference stations
ES33	29.77	95.70	67.1	0.6	10	3,7,11,12,14,15,30,38
ES34	29.91	95.47	84.8	1.2	20	3,4,7,8,10,11,12,14,15,16,36,38
ES35	29.96	94.78	111.9	1.1	09	1,4,10,14,15,16,31,36,38
ES36	29.81	93.91	86.2	1.1	13	1,4,5,7,8,11,13,14,15,38,40,41
ES37	29.90	93.51	80.5	1.4	07	1,10,13,36,39,40,41
ES38	30.02	92.97	72.5	1.2	18	3,4,5,7,8,10,11,12,36,39,40,41
ES39	29.87	92.62	75.8	1.6	17	1,2,3,4,8,9,10,11,36,38,40,41
ES40	29.71	92.15	78.0	1.4	14	1,2,4,5,7,8,10,36,38,39,41,43
ES41	29.19	91.76	70.4	1.7	14	2,3,4,5,36,38,40
ES42	28.90	91.94	108.6	1.6	06	1,37,39
ES43	29.04	92.23	75.4	1.2	05	8,36,38,39
ES45	29.12	93.78	65.8	1.3	05	7,8,38
ES46	29.25	94.26	89.2	1.1	04	10,36

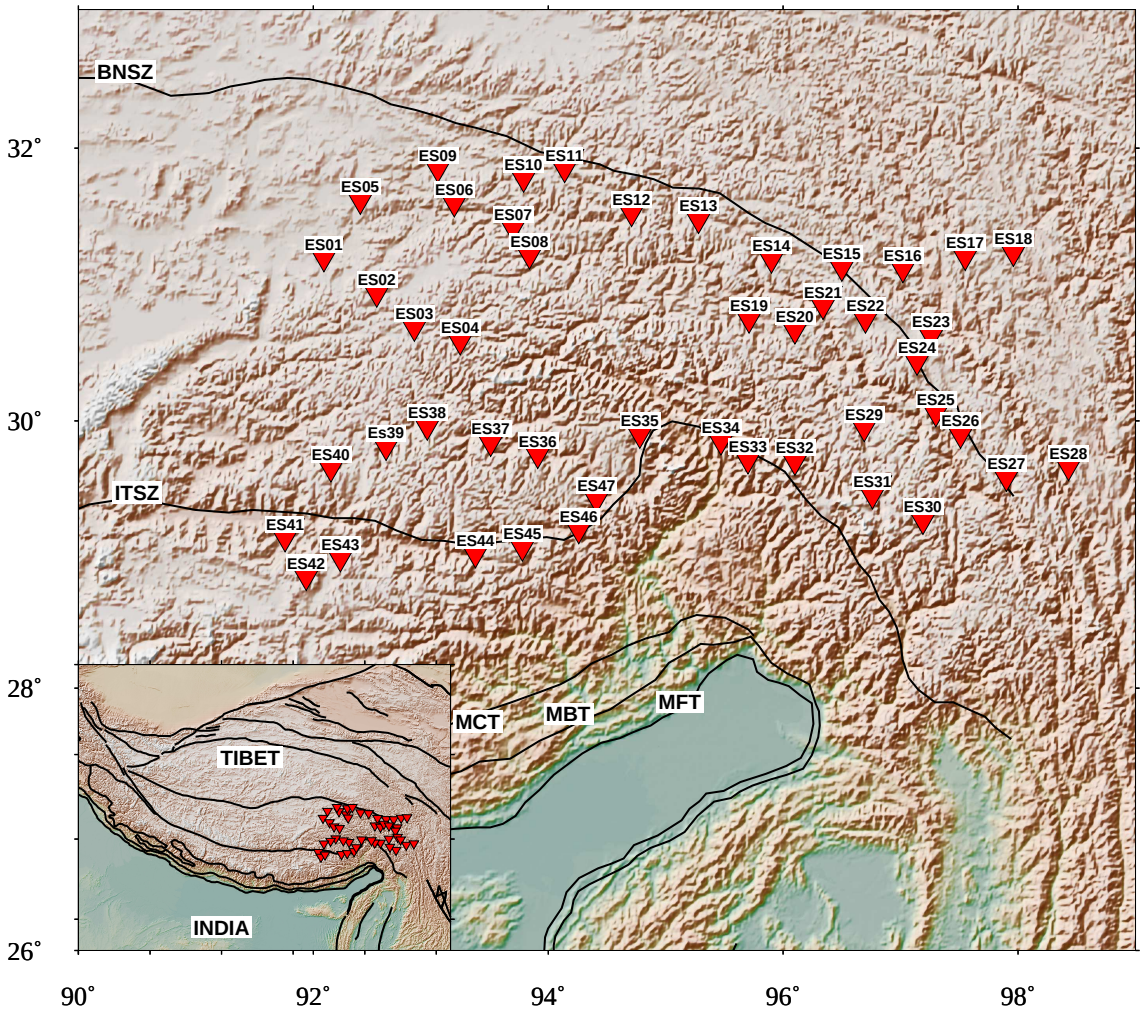

Figure 1. Tectonic and topographic map of Himalaya and Tibet. Red triangles represent the broadband seismic stations of the XE network within the study region (MFT: Main Frontal Thrust; MBT: Main Boundary Thrust; MCT: Main Central Thrust; ITCZ: Indus-Tsangpo Suture Zone; BNSZ: Bangong-Nujiang Suture Zone).

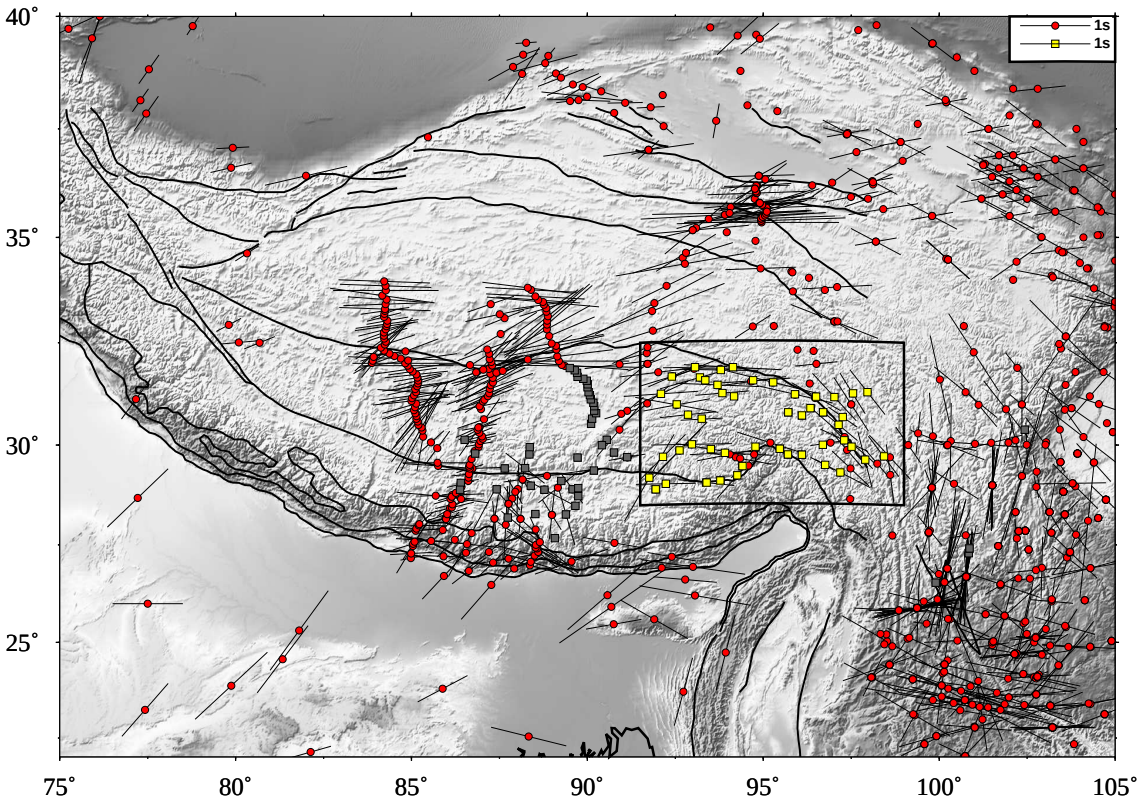

Figure 2. Earlier SKS/SKKS measurements in the study area (Sol et al., 2007; Wüstefeld et al., 2008). The length of solid bars shown each seismic station is proportional with the splitting time delay (δt_s) and their orientation represents the fast polarization direction (ϕ_s). For clarity, the seismic stations used in the present study are shown by yellow filled rectangles along with the SKS splitting measurements of Sol et al. (2007). Seismic stations where null or negligible anisotropy reported in earlier studies (see Wüstefeld et al., 2008) are shown by gray filled rectangles.

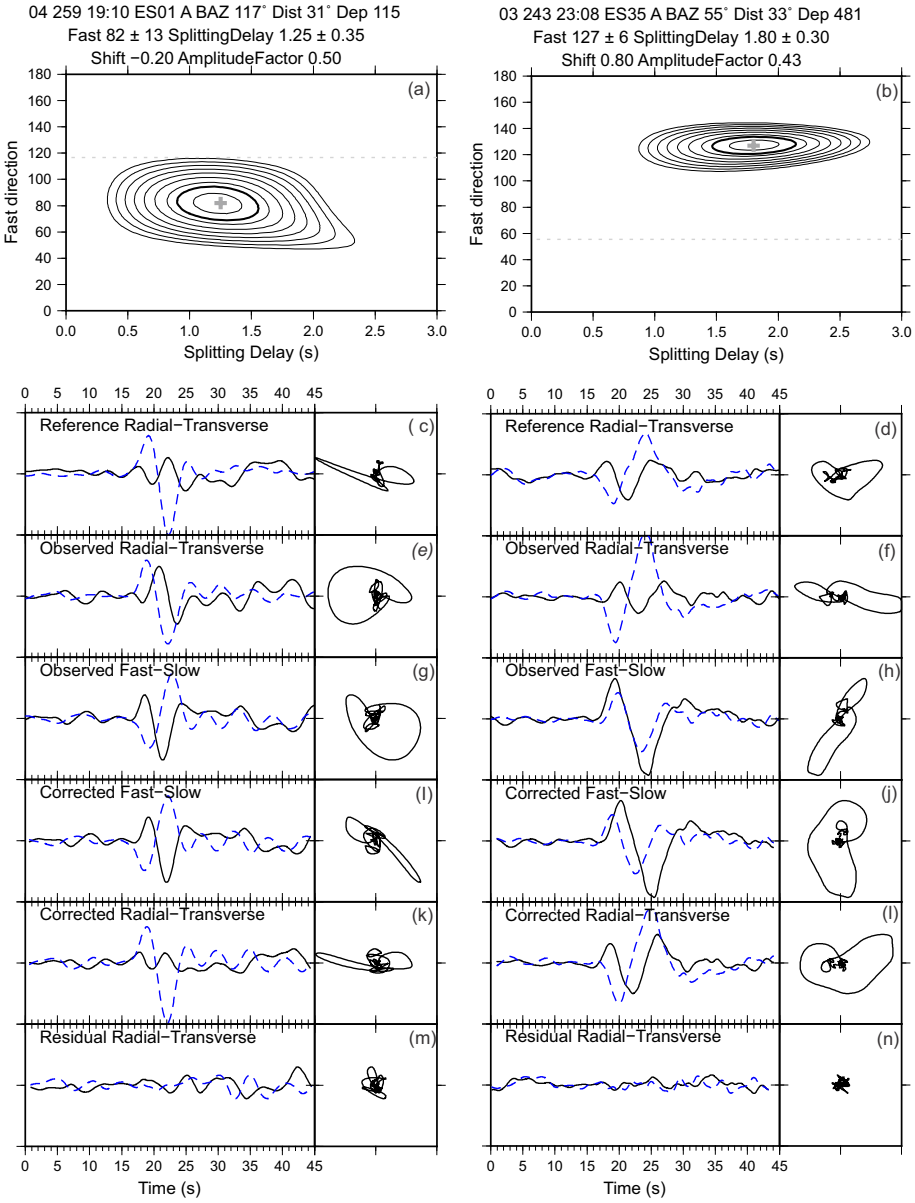

Figure 3. Examples of the direct-S waves splitting measurements based on the Reference Station Technique at stations ES01 and ES35. Figures on the left panel represent the splitting measurement recorded at station pair ES03 (reference station) - ES01 (target station) and on the right panel represent the splitting measurement recorded at station pair ES16 (reference station) - ES35 (target station). (a) Misfit surface with splitting parameter $82^\circ \pm 13^\circ$ and 1.25 ± 0.35 s. (c) signal at reference station (ES03) with receiver side correction. (e) signal at target station (ES01). (g) fast and slow component after rotating signal at target station (ES01) using ϕ (82°). (i) fast and slow component corrected for δt (1.25s). (k) corrected radial and transverse components at target station (ES01) using optimum ϕ and δt and isotropic delay (-0.2s). (m) residual trace. Figures on the right panel follow similar order and explanation.

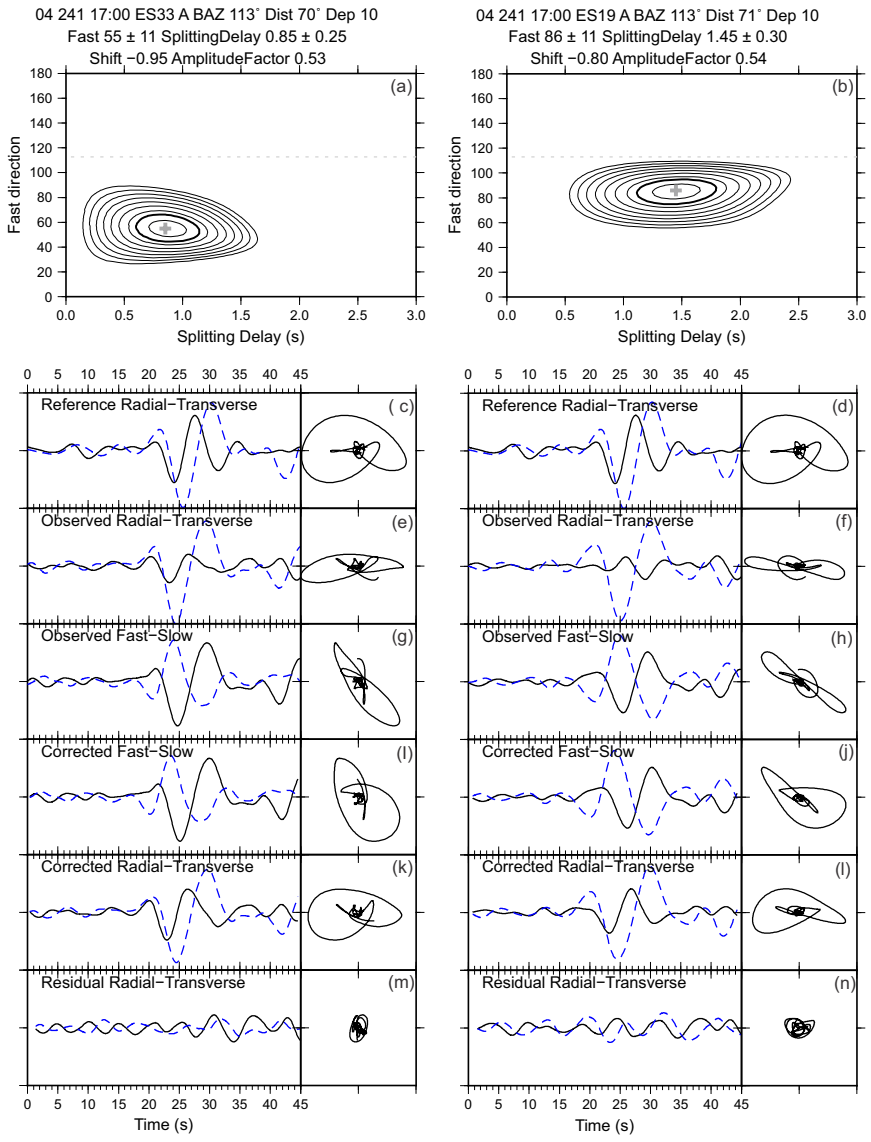

Figure 4. Examples of the direct-S waves splitting measurements based on the Reference Station Technique at stations ES33 and ES19, where previously null anisotropy was obtained using SKS splitting measurement (Sol et al., 2007). Figures on the left panel represent the splitting measurement observed at the station pair with ES12 (reference station) and ES33 (target station) and on the right panel represent the splitting measurement observed at the station pair with ES12 (reference station) and ES19 (target station). Explanation for each panel is same as in Figure 3.

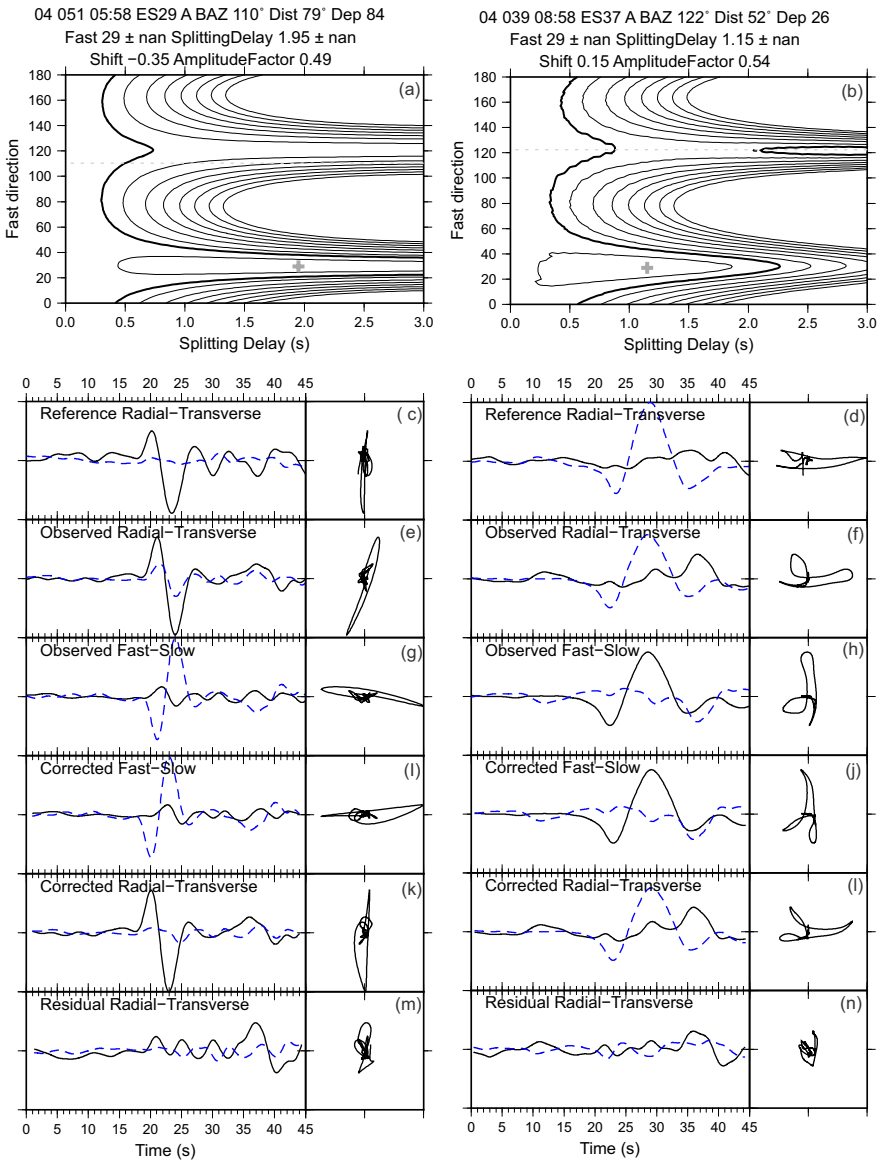

Figure 5. An examples for null anisotropic measurement based on the RST at stations ES29 and ES37. Figures on the left panel represent the splitting measurement recorded at station pair ES27 (reference station) - ES29 (target station) and on the right panel represent the splitting measurement recorded at station pair ES05 (reference station) - ES37 (target station). Explanation for each panel is same as in Figure 3.

Figure 6. Epicentral distribution of teleseismic earthquakes used in the study (30°-90°). Rectangles indicate seismic stations in this study.

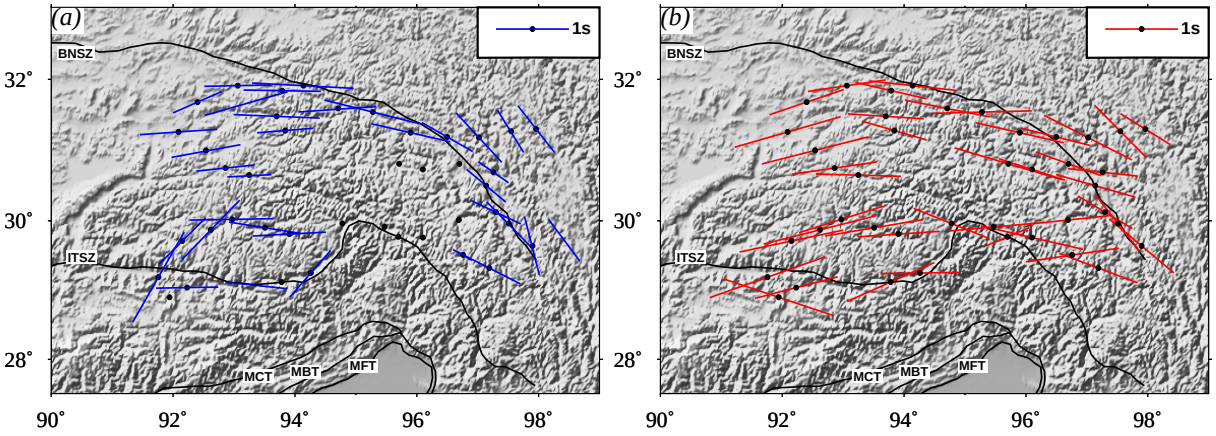

Figure 7. The tectonic and topographic map of the Southeastern Tibetan region that represents the station average splitting parameters: (a) The previous SKS-derived splitting measurements (solid blue bar) performed by Sol et al. (2007), and (b) the direct S-waves derived splitting measurements (solid red bar, this study). The length of the solid bars in each panel indicates the strength of anisotropy and is scaled by station averaged splitting time delays. Azimuth of the solid bars indicates the fast polarization direction (FPD). Black circles shows location of the seismic stations used in this study. (MFT: Main Frontal Thrust; MBT: Main Boundary Thrust; MCT: Main Central Thrust; ITCZ: Indus-Tsangpo Suture Zone; BNSZ: Bangong-Nujiang Suture Zone).

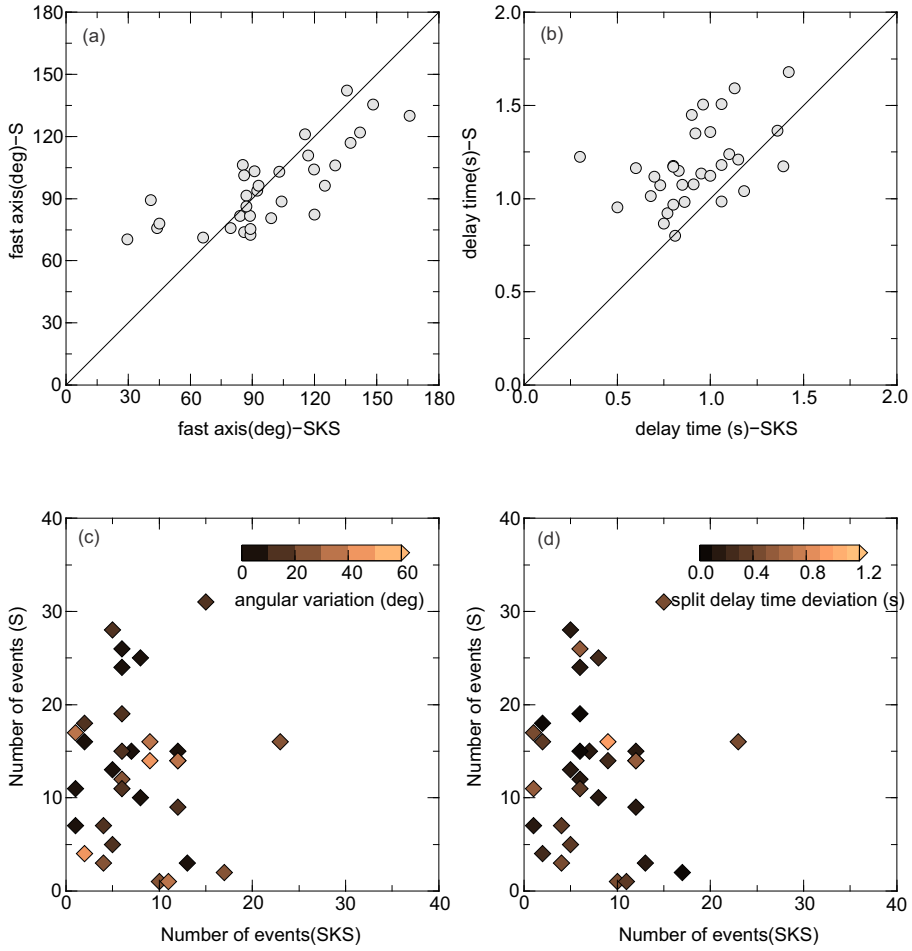

Figure 8. Comparison of SKS and S-waves derived station averaged splitting parameters in the study region. (a) and (b) Scatter plots that compare SKS and S-derived FPDs and split TDs, respectively. (c) Scatter plot of the number of individual SKS splitting measurement and the number of events used in direct S- splitting measurement (this study). Note that each station here is color coded by its absolute deviation value that is obtained by subtracting S and SKS derived FPDs. (d) The same plot for the misfit between SKS and S-derived station averaged split TDs. Average SKS splitting parameters used in this figure are taken from Sol et al. (2007).

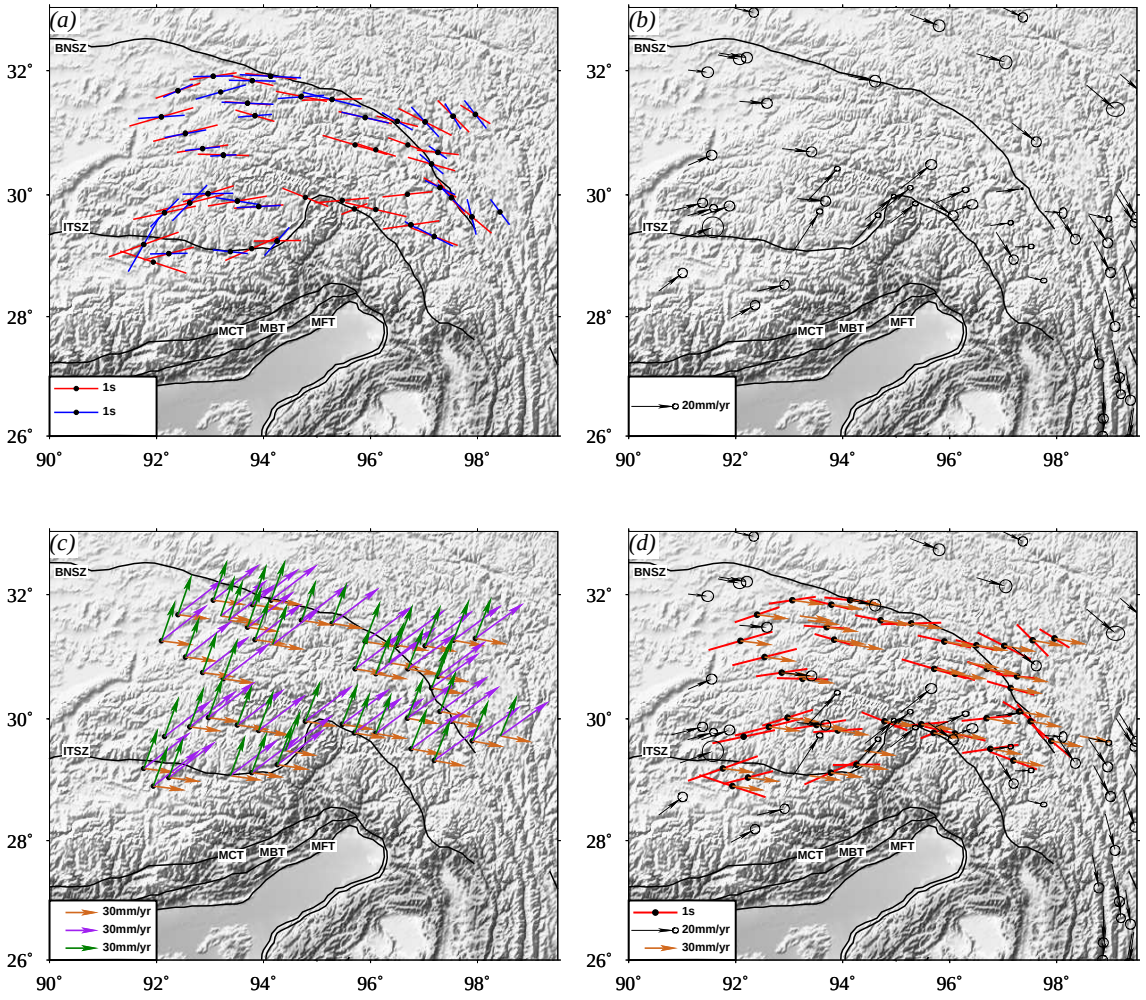

Figure 9. Lateral variations of anisotropic, geodetic, absolute plate motion data shown over topographic and tectonic features of the study area. (a) Map view comparison between the splitting measurement inferred from direct-S waves (this study shown by red bars) and SKS splitting measurements (Sol et al., 2007, in blue bars). (b) The Global Positioning System (GPS) velocity (mm/yr) vectors (black arrows) around SE Tibetan region calculated with respect to the South China reference frame and stable Eurasia. GPS data is compiled from several studies including Chen et al. (2000); Zhang et al. (2004); Shen et al. (2005); Sol et al. (2007). (c) Absolute plate motion (APM) velocities calculated through https://www.unavco.org/software/geodetic-utilities/plate-motion-calculator/platemotion-calculator.html by using GSRM v1.2 (2004) model of Kreemer et al. (2003). Note that arrows in brown, green, and purple represent the APM velocities of the Eurasian plate in no net rotation frame, of the Indian plate with respect to the Eurasian plate, and the motion of the Indian plate in no net rotation frame, respectively. (d) Map view comparisons of the station (black circle) average direct S-waves derived splitting parameters with GPS velocity (black arrow) and APM (brown arrow) vectors. Abbreviations on the maps correspond: MFT: Main Frontal Thrust; MBT: Main Boundary Thrust; MCT: Main Central Thrust; ITCZ: Indus-Tsangpo Suture Zone; BNSZ: Bangong-Nujiang Suture Zone; JRSZ: Jinsa River Suture Zone.